Reprinted from JOURNAL OF APPLIED METEOROLOGY, Vol. 35, No. 10, October 1996
American Meteorological Society

Vertical Profiles of Aerosol and Radiation and the Influence of a Temperature Inversion: Measurements and Radiative Transfer Calculations

M. WENDISCH AND S. MERTES

Institute for Tropospheric Research, Leipzig, Germany

A. RUGGABER

University of Munich, Munich, Germany

T. NAKAJIMA

Center for Climate and System Research, University of Tokyo, Tokyo, Japan

(Manuscript received 24 April 1995, in final form 11 November 1995)

ABSTRACT

The results of an airborne experiment performed near Mönchengladbach (Germany) in November 1993 are reported. Besides meteorological data, vertical profiles of aerosol properties (number concentration, size distribution) and radiation (downwelling solar and UV irradiance, JNO_2 photolysis frequency) under cloudless conditions are presented, and the influence of a strong temperature inversion is studied.

From the measured vertical profiles of the aerosol size distribution, single-scattering properties of the particles (volume scattering coefficient, asymmetry parameter, backscattering ratio) are calculated.

On the basis of the aerosol and meteorological measurements, detailed radiative transfer calculations are performed in order to model vertical profiles of the downwelling UV irradiance and JNO_2 photolysis frequency. The data of the calculated UV irradiance mostly agree with the measured values within the range given by the measurement errors. Introducing moderate absorption into the model improves the agreement. For the JNO_2 photolysis frequency there are some differences. However, the strong influence of an enhanced number of optically efficient aerosol particles below a temperature inversion on downwelling radiation could be shown for the UV irradiance as well as for the JNO_2 photolysis frequency by the measurements and the calculations.

1. Introduction

Aerosol particles influence the transfer of shortwave radiation through the atmosphere (Grassl 1988). As the solar radiation is the only relevant source of energy for the climatic system, all factors influencing solar radiation within the atmosphere are of importance for climate studies. Atmospheric aerosol particles are increasingly accepted to be an important factor affecting climate (cf. Charlson and Wigley 1994). Therefore, it is necessary to understand the interaction between aerosol particles and the respective shortwave radiative quantities.

In order to investigate the aerosol–radiation interaction, an airborne experiment under cloudless conditions has been performed, in which (beside meteorological parameters) vertical profiles of the major microphysical properties of the aerosol particles were measured under the influence of a strong temperature inversion. These parameters are used as input for a detailed radiative transfer model to predict the vertical distribution of shortwave radiative quantities such as UV irradiance and JNO_2 photolysis frequency that were recorded simultaneously during the flights.

Some examples of comparisons between measured and modeled radiative quantities are known from the literature. Tanaka et al. (1990) compared relative values (normalized) of downward measured and calculated irradiance profiles over an urban region. Introducing a reasonable absorption (absorption index of aerosol refractive index between $0.005i$ and $0.014i$) into their model calculations yielded good agreement with the measurements. The aerosol size distribution used for the model calculations was indirectly retrieved by aureole measurements of scattered solar radiation and not directly measured. Kilsby (1990) also did not use direct aerosol measurements to calculate the radiation field. Instead, he based his calculations on three standard aerosol models. The modeled downwelling diffuse fluxes are systematically underestimated because the authors utilized the delta-Eddington approx-

Corresponding author address: Dr. Manfred Wendisch, Institute for Tropospheric Research, Permoserstr. 15, 04303 Leipzig, Germany.

imation for radiative transfer, which has some problems handling highly asymmetric aerosol phase functions. The upwelling fluxes agree well with the calculations. Saunders et al. (1992) used different radiation codes to model the measured fluxes in three spectral ranges. The measured upwelling fluxes were in reasonably good agreement with the predicted ones (6 W m^{-2} maximum difference, that is, 2%). The modeled downwelling shortwave fluxes were systematically 2%–4% higher than those measured by aircraft. The authors emphasized the high sensitivity of the measured irradiance with respect to the orientation of the instruments. They conclude that major experimental efforts are needed to correct the downwelling fluxes for attitude (pitch and roll) and heading of the aircraft. Furthermore, they showed that it is important to check the alignment between sensor and aircraft plane by means of in-flight calibration techniques. However, this comparison was restricted to relatively broad spectral ranges. No measured aerosol properties were implemented into the model calculations, and no vertical profiles were investigated.

Van Weele and Duynkerke (1993) and de Arellano et al. (1994) achieved good agreement between actinic flux measurements and model calculations under total overcast conditions. No comparison was given for the cloudless case. The authors also used a delta-Eddington approximation for the radiative transfer modeling. Ruggaber et al. (1994) utilized a matrix operator model to study photochemical processes within and outside clouds. They concluded that good agreement between measurement and calculation can only be obtained with accurate and detailed input information and that the vertical profile of the aerosol properties is of particular importance, especially under cloudless conditions.

The work done in the past in this field suffers from two facts: the use of simplified radiative transfer models and/or unrealistic aerosol treatment in the models. In this contribution, detailed aerosol and radiation measurements are combined with exact radiative transfer calculations. This results in good agreement between calculated and measured UV irradiances. The weather situation chosen for the analyzed incident was characterized by a strong temperature inversion. Thus, the influence of an enhanced aerosol concentration on radiation below a temperature inversion could be investigated. In addition, vertical profiles of aerosol single-scattering properties (volume scattering coefficient, asymmetry parameter, backscattering ratio) based on the aerosol measurements are presented.

2. Experiment

An airborne experiment near Mönchengladbach was performed between 24 and 26 November 1993. Mönchengladbach is situated in the highly industrialized Ruhr area (51.2°N, 6.4°E) in the western part of Germany. During the third day (26 November 1993) of the campaign we had perfect cloudless conditions. Therefore, this day was chosen for a detailed case study. Several flight patterns were performed on 26 November 1993. The data of one of the vertical flight patterns are shown as representative results for this day.

A typical wintery high pressure situation with a stable layer of cold air near the ground was present on 26 November 1993. This situation caused a strong and permanent temperature inversion, resulting in distinct vertical differences of aerosol properties below and above the inversion, which were supposed to affect the radiation field.

A small research aircraft (Piper Chieftain Navajo) was used for our study. Its capabilities are summarized by Maser et al. (1994). The average speed of the aircraft was mostly in the range between 60 and 70 m s^{-1}. The aircraft reached a maximum altitude between 3 and 4 km.

Temperature and humidity measurements were made with Vaisala sensors in a reverse flow inlet system. The static pressure was supplied by a Pitot sonde. The geographical coordinates, which are essential to correct the radiation measurements, were measured by a GPS. (All acronyms used in this paper are explained in the appendix.) The heading of the airplane was calculated from geographical data. The pitch and roll angles of the aircraft were obtained from a gyroscope compass (INS).

Table 1 gives an overview of the microphysical and radiation equipment onboard the aircraft. Some comments on the instrumentation are given below.

a. *Microphysical measurements*

The ambient aerosol particles were sampled by an aerosol inlet developed by Maser et al. (1994), which assured isokinetic sampling for a flight velocity of about 64 m s^{-1}. The inlet was equipped with an internal impactor with an cut off diameter of 5 μm.

The concentration of aerosol particles with diameters larger than 0.01 μm were determined by a TSI-3010 CPC (TSI, Inc., St. Paul, Minnesota). The raw counts were converted into concentrations applying a statistical coincidence correction.

TABLE 1. List of instrumentation: D—diameter of aerosol particles, λ—wavelength.

Instrument	Specification	Measured quantity
Microphysics		
TSI-3010 CPC	$D > 0.01$ μm	Aerosol concentration
PCASP-X	$D = 0.1-10$ μm	Aerosol size distribution
Radiation		
PSP	$\lambda = 0.3-3$ μm	Solar irradiance ↓
TUVR	$\lambda = 0.3-0.4$ μm	UV irradiance ↓
JNO_2 detector	$\lambda = 0.3-0.4$ μm	Photolysis frequency of NO_2 ↓

The size distribution of the aerosol particles (accumulation mode and coarse particles) was determined by a laser aerosol spectrometer (PCASP-X, PMS, Inc., Boulder, Colorado). The 31 size channels characterize the aerosol size distribution from 0.1 to 10 μm according to their dry diameter. During the flights under consideration, the ambient relative humidity outside the aircraft was below 60%. The major growth of the common hygroscopic components of aerosol particles starts well above 60% relative humidity (Tang and Munkelwitz 1993); therefore, the drying of the aerosol particles by the sampling procedure did not drastically change the ambient particle size. Therefore, no humidity correction was applied to the data. The measurements of the PCASP-X were activity corrected corresponding to the manual of the manufacturer. During the analyzed flights, the values of the activity parameter varied from 10% near the ground and about 3% above 1-km altitude.

The instrument was calibrated using a Mie curve adjustment procedure. For this purpose, the PHA threshold settings of the PCASP-X are adapted to the Mie scattering curve, which describes the scattering response of the instrument theoretically. The Mie scattering cross section C_{sca} is a measure of the intensity of the scattered laser light caused by a particle of given refractive index n and diameter D. For the PCASP-X we obtain

$$C_{sca}(n, D) = \frac{\lambda^{*2}}{4\pi} \int_{\psi_1}^{\psi_2} [j_1(n, D, \lambda^*, \psi') + j_2(n, D, \lambda^*, \psi')] \sin\psi' d\psi', \quad (1)$$

where $\lambda^* = 0.6328$ μm is the wavelength of the laser of the PCASP-X, j_1 and j_2 are scattering functions of single particles (dimensionless), and ψ is the scattering angle (°). The single-scattering functions for parallel and perpendicular polarized light j_1 and j_2 were calculated via Mie theory (cf. Bohren and Huffman 1983). The integration includes the angular range of the PCASP-X from $\psi_1 = 45°$ to $\psi_2 = 135°$.

For a suitable adjustment of the PHA threshold voltages to the Mie curve, the following three steps (a)–(c) were realized. We illustrate this technique for the gain range 3 of the PCASP-X, which covers the size range from 0.3 to 0.9 μm. For the other gain ranges the procedure is similar.

(a) Monodisperse latex particles were supplied to the instrument and the respective counts indicated by the PCASP-X were recorded. For gain 3 we have used latex particles of 0.629-μm diameter. The channel number l_{lat} with the maximum counts was recorded with 1-s time resolution. Because the latex particles are not perfectly monodisperse, l_{lat} may not be singular, therefore, an average value $\langle l_{lat} \rangle$ was calculated, which was used to find the corresponding average voltage $\langle U_{lat} \rangle$ by linear interpolation of the neighboring PHA threshold voltages.

(b) Then the scattering cross section C_{lat} for the latex beads

$$C_{lat} = C_{sca}\,(n = n_{lat} = 1.588 - 0i,\, D = 0.629\ \mu\text{m})$$

was calculated from Eq. (1). This value C_{lat} was used to find a scaling factor K, which relates the voltage (mV) of the PHA to the scattering cross section (cm^{-2}) of the monodisperse latex particles;

$$\langle U_{lat} \rangle = K C_{lat}.$$

Now it is possible to plot the PHA threshold voltages and the scattering cross section of latex particles of different size on a common diameter scale, which was done in Fig. 1a.

(c) It is obvious from Fig. 1a that the PHA threshold voltages do not optimally correspond to the Mie scattering curve for latex particles. Furthermore, the refractive index of atmospheric aerosol particles is different from that of latex spheres. Therefore, the PHA threshold voltages were related to the Mie scattering curve of a refractive index, which is typical for ambient aerosol particles. We have used the refractive index of ammonium sulfate ($n_{sul} = 1.525 - 10^{-7}i$). This is justified by the calculations performed in section 4b, which showed that the radiation measurements are well reproduced using a real part of refractive index of 1.525. Then the size channels of the fixed PHA threshold voltages were shifted in a way that they correspond to the Mie scattering curve of ammonium sulfate. Figure 1b shows the result of this procedure. The effects of the matching procedure were largest for the smaller particles and reached values up to 10%.

From the corrected data (activity, Mie curve adjustment), the logarithmic number size distribution (cm^{-3}) is calculated by Eq. (2):

$$\frac{dN}{d\log_{10}D} = \left(\frac{\Delta D_i}{2} + D_i\right) \ln 10 \frac{N_i}{\Delta D_i}, \quad (2)$$

where N_i represents the activity corrected measured number concentration of aerosol particles (cm^{-3}) in size bin i ($i = 1, 31$). The values $\Delta D_i = D_{i+1} - D_i$, $i = 1.31$ correspond to the diameter bins obtained by the Mie curve adjustment procedure.

From the integral of the number size distribution, the total number concentration (cm^{-3}) of the aerosol particles for the size range covered by the PCASP-X (0.1–10 μm) is calculated. Furthermore, the logarithmic volume size distribution is obtained by Eq. (3):

$$\frac{dV}{d\log_{10}D} = \frac{\pi}{6} D^3 \frac{dN}{d\log_{10}D}. \quad (3)$$

b. Radiation

1) IRRADIANCE

Two upward looking sensors (PSP and TUVR, cf. Table 1) were installed onboard the aircraft to measure

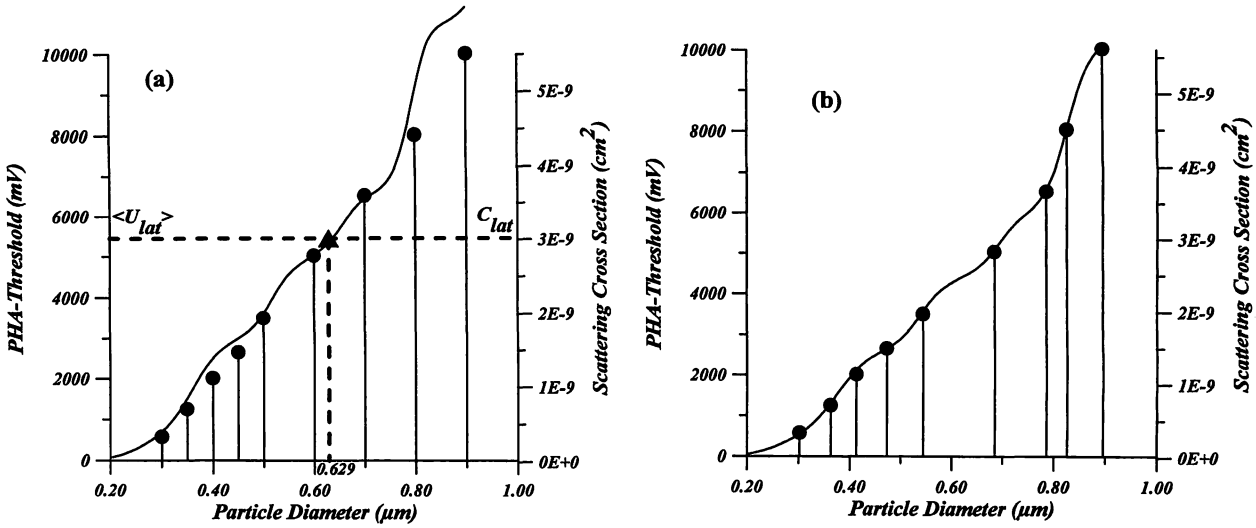

FIG. 1. PHA threshold voltages (bars with dots, left scale) and scattering cross section C_{sca} (solid curve, right scale) versus particle diameter D. (a) The threshold bars are related to the diameters given by the manufacturer. The refractive index of latex particles $n_{lat} = 1.588 - 0i$ is used in the calculations of C_{sca}. The triangle represents the calibration point for scaling. (b) The threshold bars are shifted to diameters matching the Mie curve for ammonium sulfate, with $n_{sul} = 1.525 - 10^{-7}i$.

the downwelling radiation flux density onto a horizontal plane (i.e., irradiance) in two different wavelength ranges. Corrections considering the actual aircraft attitude and relative position of the aircraft with respect to the sun were performed according to Bannehr and Glover (1991). The sun position was calculated using the equations given by Iqbal (1983). The direct component of the measured total irradiance (direct plus diffuse) was corrected for aircraft attitude. For this purpose the ratio between direct and total irradiance was estimated by in-flight experiments as well as model calculations.

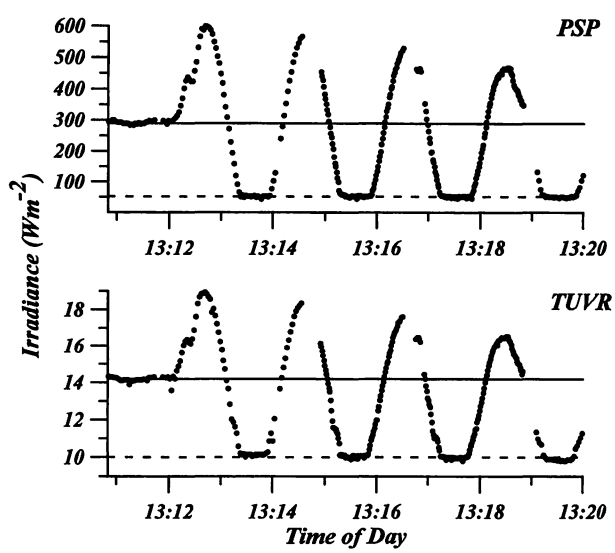

FIG. 2. Measurements of solar (PSP) and UV (TUVR) irradiance during a circle flight on 26 November 1993 near Mönchengladbach, Germany, in order to determine the ratio between direct and diffuse irradiance. Altitude is about 3 km.

An example of the in-flight calibration measurements is given in Fig. 2, in which the data of PSP and TUVR are plotted during horizontal circle patterns of the aircraft at 3-km altitude. The roll angle was constant, the pitch angle was zero during the maneuver. When the sensors were shadowed by the aircraft fuselage during the circle patterns, the measured values of PSP and TUVR reached a stable minimum (dashed curves in Fig. 2). Assuming isotropic radiation, this minimum represented the diffuse irradiance. The total irradiance was obtained from the horizontal flight leg just before the circles (solid lines in Fig. 2). Thus, the ratio of direct to total irradiance $r = F_{dir}/F_{tot}$ was calculated to be $r_{PSP} = 0.80 \pm 0.05$ for the PSP and $r_{TUVR} = 0.30 \pm 0.05$ for the TUVR, respectively. The value for the TUVR sensor is smaller because increasing multiple scattering with decreasing wavelength raises the diffuse part of radiation.

Because solar radiation is highly anisotropic, the in-flight determination of the diffuse irradiance by circle patterns is uncertain. Therefore, spectral model calculations of r were performed in order to support the results of the measurements. The input data and the model itself are explained in section 4b. As a result, the measured values of both the PSP and the TUVR agreed well with these model calculations of r. Furthermore, the calculations have proven that the height dependence of r is negligible for the final irradiances.

Any misalignment between the horizontal planes of the radiation sensors with respect to the airplane causes additional uncertainties. In order to check and correct

the data for misalignment, an in-flight calibration technique was performed, which was similar to that proposed by Bannehr and Schwiesow (1993). It consisted of a horizontal triangle flight pattern at constant height level. During the flight legs, the measured downwelling irradiances are expected to stay constant. If the sensors are misaligned, the radiation level will change between the flight legs. The in-flight calibration measurements yielded the following results for the misalignment of the roll angle $\Delta\alpha$ and the pitch angle $\Delta\beta$ for the irradiance sensors used in our study:

$$\text{PSP:} \quad \Delta\alpha = -1.2°, \quad \Delta\beta = +0.2°$$

$$\text{TUVR:} \quad \Delta\alpha = -1.2°, \quad \Delta\beta = -1.0°.$$

2) JNO_2 PHOTOLYSIS FREQUENCY (UV ACTINIC FLUX)

The UV actinic flux (W m^{-2}) is defined as the radiation flux density related to the surface of a unit sphere (cf. Demerjian et al. 1980). This quantity is important for photochemical processes in the cloudless sky as well as within clouds (cf. Finlayson-Pitts and Pitts 1986). The instrument used in this study measures the photolysis frequency of NO_2, J_{NO_2}, which is linked to the spectral actinic flux $F_A(\lambda)$ by Eq. (4) (cf. Madronich 1987):

$$J_{NO_2} = \int_0^\infty \varphi_{NO_2}(\lambda)\sigma_{NO_2}(\lambda)F_A(\lambda)d\lambda, \qquad (4)$$

where φ_{NO_2} is the quantum yield of NO_2 and σ_{NO_2} is the absorption cross section of NO_2. Because the wavelength dependence of φ_{NO_2} and σ_{NO_2} between $\lambda = 0.3$ and 0.4 μm is weak, an approximately linear relationship between the integrated actinic flux and the photolysis frequency of NO_2 exists. Thus, the measurement of J_{NO_2} gives a qualitative measure of the actinic flux in the atmosphere (between 0.3- and 0.4-μm wavelength).

The details of the measurement principle of our JNO_2 detector are given in Junkermann and Platt (1989). A commercial version of this instrument was used in our experiments (Meteoconsult GmbH, Glashütten, Germany).

3. Experimental results

a. Vertical aerosol profiles

1) AEROSOL PARTICLE NUMBER CONCENTRATION

Figure 3 shows the vertical distribution of the aerosol number concentration measured by the TSI-3010 CPC and the PCASP-X. In addition, the temperature is plotted in Fig. 3, which shows two distinct inversion layers (marked with arrows 1–4). The arrow indications are used in the following figures, respectively. In general, the CPC concentrations were considerably higher than those detected by the PCASP-X, indicating that there

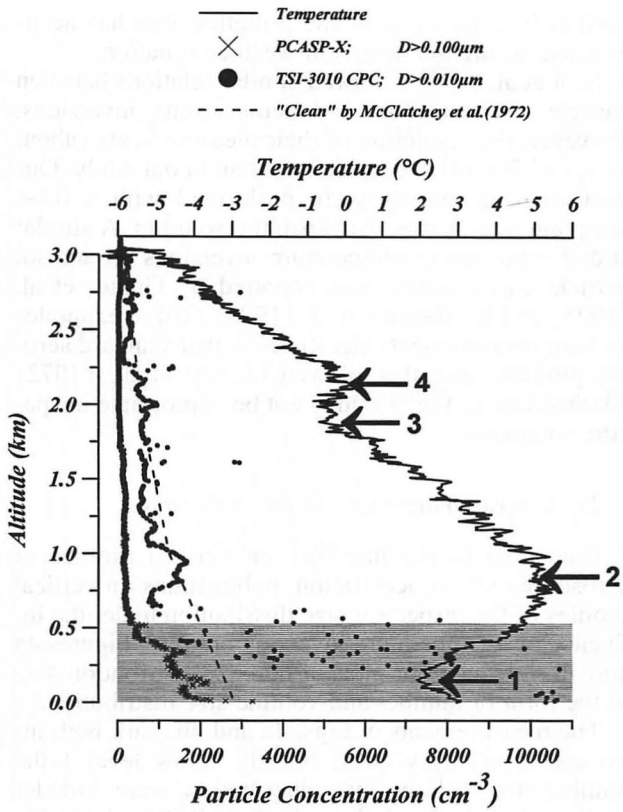

FIG. 3. Vertical profiles of temperature (solid line, upper scale) and particle concentrations (lower scale) measured by the TSI-3010 CPC (dots) and the PCASP-X (crosses) measured during a vertical flight pattern on 26 November 1993 near Mönchengladbach, Germany. The dashed line represents the standard profile from McClatchey et al. (1972), type "clean."

was a considerable amount of nucleation mode particles with diameters smaller than 0.1 μm. Furthermore, the difference between CPC and PCASP-X concentrations decreased strongly with altitude.

Just below the lower temperature inversion (arrow 1), a strong maximum of particle concentrations was recorded by both instruments. Note that the CPC was mostly in saturation below level 1. In the stable layer between the levels 1 and 2, the particle concentration decreased, demonstrating that the inverted temperature profile hinders the vertical exchange. The layer below 530-m altitude contained the majority of the optically efficient accumulation mode particles (PCASP-X size range). Therefore, this layer was hatched and this indication is kept in the following figures.

In the layer between arrows 2 and 3, the concentration of the aerosol particles measured by the CPC and PCASP-X is low and more or less constant, indicating that this layer is well mixed. The second inversion (between arrows 3 and 4) was not detected in either the CPC or the PCASP-X concentration data because the particle source was near the ground and the lower in-

version blocked most of the pollution that has accumulated during the inversion weather situation.

Foot et al. (1985) showed similar relations between particle concentration and temperature inversions. However, the resolution of their measurements (about 10 s, i.e., 700 m) was much less than in our study. Our measurements mostly were performed with a 0.1-s sampling rate, that is, 7-m spatial resolution. A similar strong influence of temperature inversions on aerosol particle concentration was reported by Gunter et al. (1993) and Kristament et al. (1993). These examples and our measurements clearly show that standard aerosol profiles, like that of McClatchey et al. (1972) (dashed line in Fig. 3), may not be appropriate in specific situations.

2) AEROSOL PARTICLE SIZE DISTRIBUTION

Compared to the literature on vertical profiles of aerosol particle concentration, publications on vertical profiles of the respective size distribution under the influence of a temperature inversion are rare. Figures 4a and 4b show contour plots of our size distribution data in the form of number and volume size distribution.

The measurements in Figs. 4a and 4b mark both inversion layers very clear. Shortly below level 1 the number and volume size distribution were broader compared to the level above layer 1. Within the stable inversion layer, a sharp decrease of the number and volume of the large particles occurred. The modal diameter of the number size distribution shifted from 0.25 to about 0.18 μm, the mean volume diameter decreased from 0.35 to about 0.29 μm. In the layer between arrows 2 and 3, the size distribution remained nearly constant due to the convective mixing in this region. In contrast to the number concentration (Fig. 3), the size and volume distribution measurements of the PCASP-X clearly indicated the second inversion between arrows 3 and 4. We conclude that the aerosol size distribution reflects the influence of a temperature inversion more obvious than simple concentration measurements.

Our measurements of the number size distribution show, similar to Kristament et al. (1993), only one mode in the accumulation size range and no coarse particle mode as reported by Kim et al. (1993).

b. *Vertical profiles of radiation*

Figure 5 summarizes the results of the measurements of the downwelling radiation by showing the normalized signals of the three radiation sensors.

It is obvious from Fig. 5 that in the layer of enhanced number of optically efficient particles (hatched area) the signals of all three instruments drastically decreased. The influence of the aerosol layer between arrows 3 and 4 was not detected.

Although much effort was put into the correction of the irradiance data, the quality of the PSP measurements was not satisfactory. The decrease of the solar irradiance in the layer of enhanced optically efficient aerosol particles was proven, but the fluctuations of the measurements were large. The most important reason for these fluctuations was the uncertainty of the aircraft's heading, which strongly influenced the direct part of the irradiance especially for the PSP sensor. The PSP has a relative long response time (about 3 s) com-

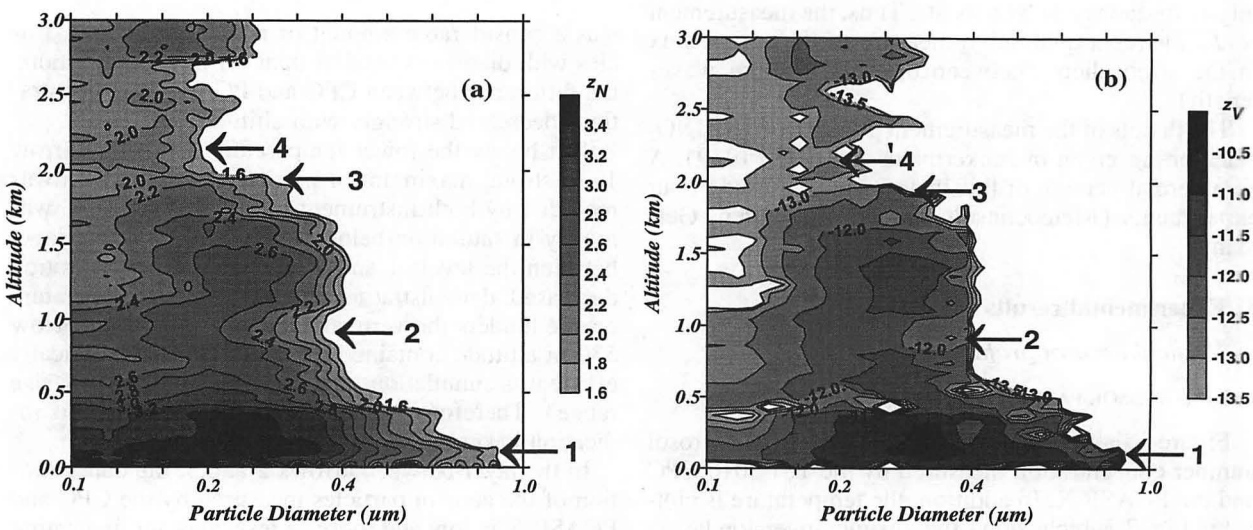

FIG. 4. Vertical profile of aerosol size distribution measured by the PCASP-X on 26 November 1993 near Mönchengladbach, Germany. (a) Contour plot of the logarithm of the *number* size distribution in the form $z_N = \log_{10}(dN/d\log_{10}D)$. Thus, the level $z_N = 3$ denotes a number concentration of 1000 particles per cubic centimeter corresponding to the logarithmic size interval. (b) Contour plot of the logarithm of the *volume* size distribution in the form $z_V = \log_{10}(dV/d\log_{10}D)$. Thus, the level $z_V = -12$ denotes an aerosol particle volume of 10^{-12} cm^3 cm^{-3} air corresponding to the logarithmic size interval.

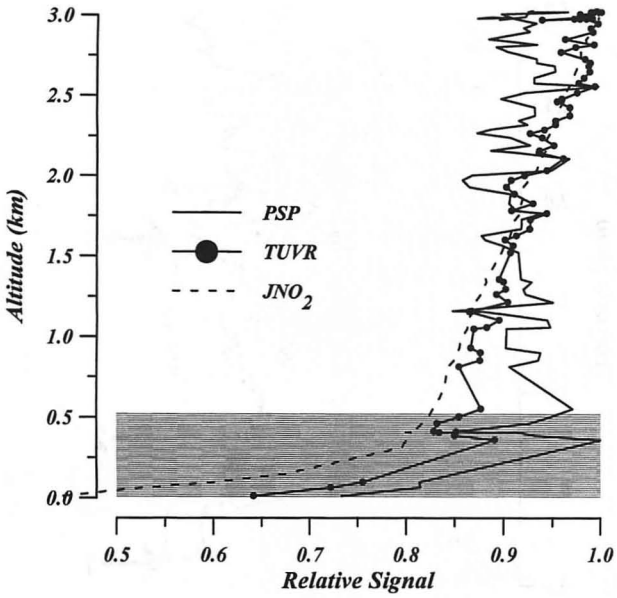

FIG. 5. Relative signals of PSP, TUVR, and JNO_2 detectors versus altitude for the ascent on 26 November 1993 nearby Mönchengladbach, Germany. The data are normalized; thus, the maximum is equal to 1.

pared to the TUVR and JNO_2 detector (in the range of milliseconds). This fact further limits the accuracy of the PSP measurements. Furthermore, it is well known that the PSP sensor is very sensitive to atmospheric temperature changes. Therefore, the PSP measurements were excluded from the further analysis.

The PSP and TUVR measurements were highly correlated because the same aircraft attitude correction procedures were applied to both data. Nevertheless, the TUVR measurements are less fluctuating because the direct part of the total irradiance is much less ($r_{TUVR} = 0.3$, $r_{PSP} = 0.8$). Furthermore, the response time of the TUVR is much faster compared to the PSP.

In the case of actinic flux measurements, no correction concerning attitude and heading of the aircraft is necessary because of the isotropic response of the sensor. This fact explains the smooth JNO_2 profile.

4. Calculations

a. Single-scattering properties of aerosol particles

On the basis of the measured aerosol number size distribution, Mie calculations were performed (cf. Bohren and Huffman 1983) in order to obtain vertical profiles of several bulk aerosol parameters such as the volume scattering coefficient and the asymmetry factor. These quantities are of interest for model studies, which cannot afford to incorporate details of the aerosol properties in the code. However, often crude assumptions on aerosol characteristics are used in the models. Furthermore, different measurement techniques require information on bulk aerosol properties for their data analysis. As an example, the analysis of Lidar data requires the backscattering ratio to deduce vertical profiles of the volume scattering coefficient of the aerosol particles (cf. Evans 1988).

In this section the vertical and spectral distribution of the following three parameters is discussed.

(a) Volume scattering coefficient of aerosol particles σ_{sp}

$$\sigma_{sp}(\lambda) = \int_0^\infty C_{sca}(n, D', \lambda) \frac{dN}{d \log_{10} D} d \log_{10} D'. \quad (5)$$

(b) Asymmetry factor of aerosol particles g

$$g = \frac{\int_{-1}^{+1} p(\psi) \cos\psi \, d \cos\psi}{\int_{-1}^{+1} p(\psi) \, d \cos\psi}, \quad (6)$$

where p is the phase function of aerosol particles, calculated from Mie theory.

(c) Backscattering ratio (also called lidar ratio) S

$$S(\lambda) = \frac{\sigma_{sp}}{\beta_{sp}}, \quad (7)$$

where β_{sp} is the volume backscattering coefficient of aerosol particles.

The Mie calculations are based on the measured aerosol size distributions shown in Fig. 4a. The refractive index of ammonium sulfate is used, which is justified by the calculations in section 5.

1) VOLUME SCATTERING COEFFICIENT OF AEROSOL PARTICLES σ_{sp}

Figure 6a illustrates an example of the vertical profiles for the volume scattering coefficient σ_{sp}. The temperature and the resulting aerosol layers are clearly reflected because the single-scattering properties follow the features of the size distribution. Consequently, a simple parameterization of the volume scattering coefficient by means of the aerosol number concentration does not work.

Arrow 1 marks the maximum of σ_{sp}. Within the stable inversion layer (between arrows 1 and 2) σ_{sp} decreased because the number of small particles decreases (Fig. 4a). The same holds for the second inversion layer between arrows 3 and 4. The increase of σ_{sp} directly above layer 2 is mainly caused by the shift of the maximum size of the particles to larger diameters (cf. Fig. 4a). Thus, the stratification of aerosol layers was clearly represented in the profile of σ_{sp}. A simple exponential decrease of σ_{sp} with altitude as often assumed in models is clearly not observed in the case of an inversion when aerosol concentrations are high and significant for radiative transfer effects.

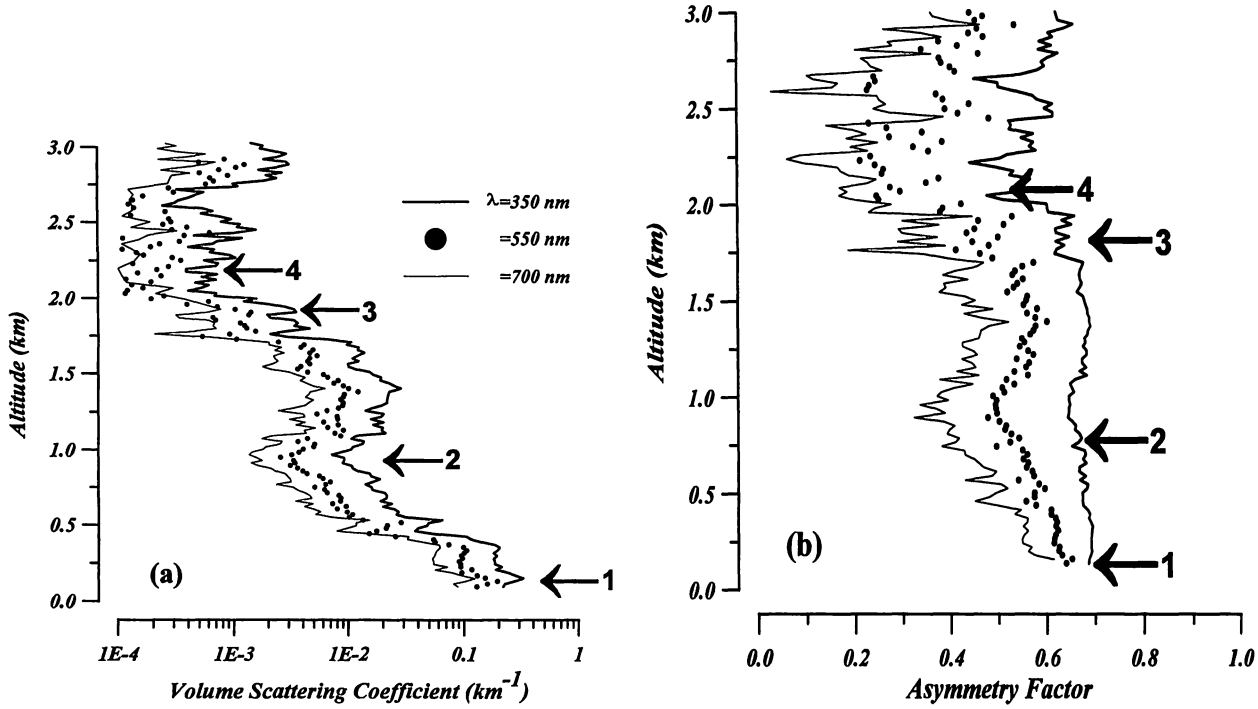

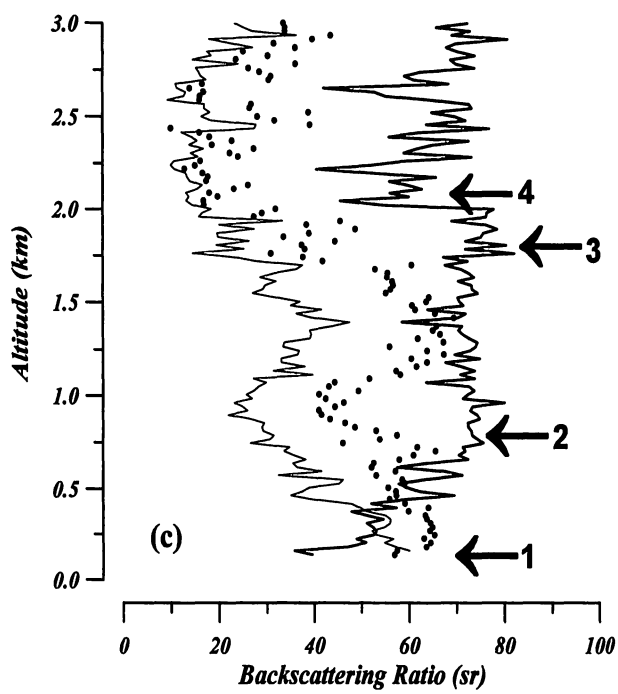

FIG. 6. Calculated single-scattering properties of aerosol particles for the ascent on 26 November 1993 near Mönchengladbach, Germany, for the three wavelengths λ = 350, 550, and 700 nm. (a) Volume scattering coefficient σ_{sp} versus altitude. (b) Asymmetry factor g versus altitude. (c) Backscattering ratio S versus altitude.

TABLE 2. Input parameters for the radiative transfer model.

Input parameter	Below 3 km	Above 3 km
Pressure, temperature, and humidity	Aircraft measurements	Type "U.S. standard" by McClatchey et al. (1972)
Aerosol concentration	Aircraft measurements	Type "clear" by McClatchey et al. (1972)
Aerosol phase function	Mie calculations using aircraft measurements of aerosol size distribution $n_{sul} = 1.525 - 10^{-7}i$	• 3–12 km: type "clean continental" • 12–100 km: type "stratospheric," Both types by d'Almeida et al. (1991)
Ground albedo	Type "grass" by Bowker et al. (1985)	Type "grass" by Bowker et al. (1985)
Ozone density profile	Type "U.S. standard" by McClatchey et al. (1972)	Type "U.S. standard" by McClatchey et al. (1972)
NO_2 density profile	Roeth (1986)	Roeth (1986)

Our data are comparable to the results of others in urban regions. Stettler and von Hoyningen-Huene (1994) obtained volume extinction coefficients near the ground between 0.05 and 0.60 km^{-1} using a laser transmission technique. Horvath (1991) found average values of 0.10 km^{-1} for the volume extinction coefficient in Europe at the ground with a telephotometer. Some studies deal with vertical profiles of σ_{sp} using integrating nephelometers. Brock et al. (1989) reported maximum values of up to 0.124 km^{-1} for σ_{sp} in Arctic haze layers. Gunter et al. (1993) showed profiles of σ_{sp} using a three-wavelength nephelometer. These profiles are similar to our measurements and are deduced from an optical particle counter.

2) ASYMMETRY FACTOR OF AEROSOL PARTICLES g

Figure 6b shows the vertical profile of the asymmetry factor g. The asymmetry of aerosol scattering decreased with increasing altitude, which is due to the decreasing number of large particles at higher altitudes. The use of a constant value for g, which is common practice in radiative transfer calculations, cannot be recommended. Especially for larger wavelengths ($\lambda > 550$ nm), the asymmetry factor varied significantly with altitude. The aerosol stratification of the atmosphere clearly influenced g. This finding again emphasizes the need of detailed size distribution measurements for radiative transfer calculations.

3) THE BACKSCATTERING RATIO S

For lidar applications S is a crucial parameter for the retrieval of vertical profiles of the aerosol volume scattering coefficient. For that purpose often height-independent values of the backscattering ratio S are assumed (cf. Evans 1988). The values given in the literature vary from 10 to 1000 sr depending on the assumptions about the aerosol type.

The results presented in Fig. 6c show that the assumption of a constant backscattering ratio S is not generally justified. Furthermore, it is obvious that there is no well-defined behavior of the altitude change of S. For small wavelengths ($\lambda < 350$ nm) the backscattering ratio increased with altitude, whereas for larger wavelengths ($\lambda > 550$ nm) this behavior was reversed. Because the backscattering ratio is directly linked to the number size distribution, both inversion layers were evident in this parameter.

b. Radiative transfer calculations

The aerosol and meteorological measurements were used in a comprehensive and detailed radiative transfer model. The one-dimensional spectral model is described by Ruggaber et al. (1994). It is based on the "matrix operator method" (cf. Nakajima and Tanaka 1986). A delta approximation with several truncation approaches for the phase function is included in the model (cf. Nakajima and Tanaka 1988). Deviations from a plane-parallel atmospheric geometry are considered in the model.

With this model we have simulated the ascent on 26 November 1993. The input data for the model are summarized in Table 2. The atmosphere from 0- to 3-km altitude was divided into 43 layers. Thus, a vertical resolution of about 70 m was achieved. Between 3 and 100 km appropriate standard values were assumed with a resolution of 30 layers. Test calculations have shown that the choice of the standard atmosphere above 3 km did not influence the boundary layer results significantly. In each of the 43 layers between 0 and 3 km, the measured aerosol size distribution was used to calculate spectral scattering and extinction coefficients of the aerosol particles and their phase function. These aerosol parameters were complemented by several gas species and their scattering and absorption properties (cf. Ruggaber et al. 1994). The meteorological parameters (pressure, temperature, and humidity) were taken from the measurements during the flight. Thus, the optical description of each layer was mainly based on a set of experimental data.

The integrated irradiance and photolysis frequency of NO_2 were calculated with an efficient spectral integration module on the basis of the spectral functions supplied by the radiation model. The spectral response of the instruments, as well as their directional sensitivity, was included in the calculations.

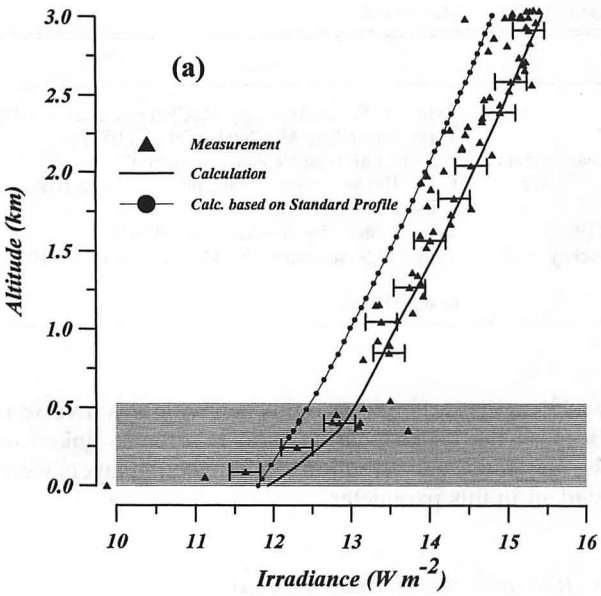

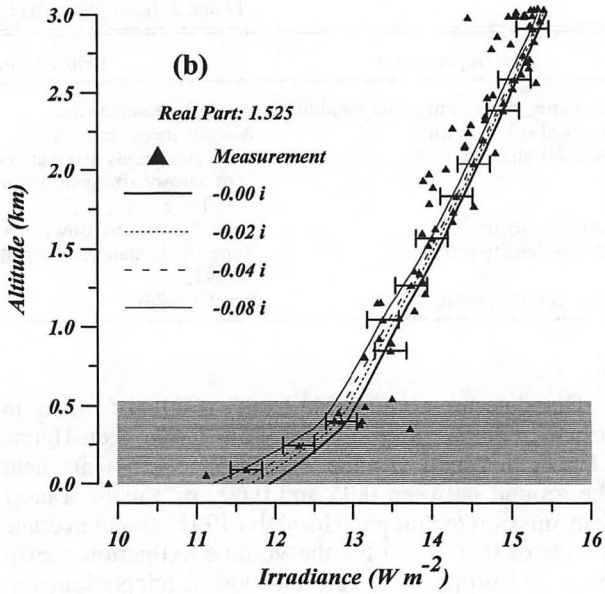

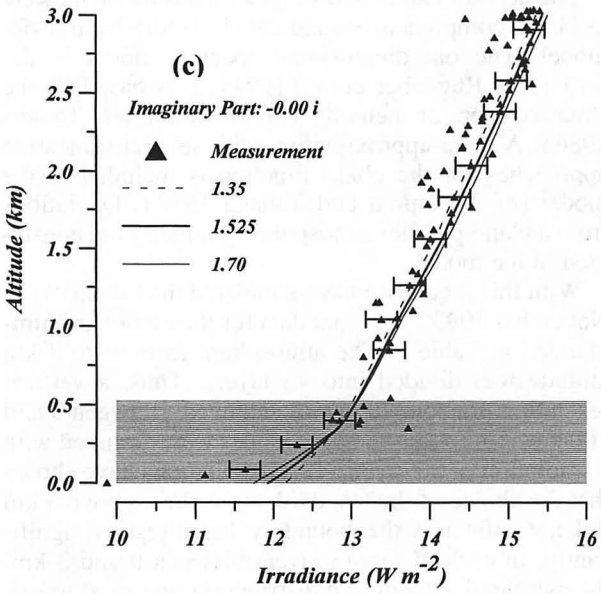

FIG. 7. UV irradiance measured by the TUVR (triangles) and corresponding calculated values versus altitude for the ascent on 26 November 1993 near Mönchengladbach, Germany. (a) The solid line shows the results of the calculations based on measured profiles of meteorological and aerosol parameters (cf. Table 2). The dotted curve represents the calculations using standard aerosol assumptions as input for the model. (b) Variation of imaginary part of aerosol refractive index from $-0.00i$ to $-0.08i$. (c) Variation of real part of aerosol refractive index from 1.35 to 1.70. (d) Variation of total ozone content from 220 to 420 DU. (e) Final result of the calculations with the refractive index $n = 1.525 - 0.03i$ and the total ozone content of 300 DU.

5. Comparison between measurements and calculations

On the basis of the measured aerosol properties, radiation profiles were calculated in order to compare the results with the measurements. In Figs. 7 and 8, measured and calculated vertical profiles of downwelling total UV irradiance (direct plus diffuse) and photolysis rates of NO_2 are plotted.

a. UV irradiance

Figure 7a shows that the calculated UV irradiances are mostly within the range of uncertainty of the measurements. Within the hatched area the particle concentration increased significantly (cf. Fig. 3), which had direct consequences for the downwelling UV irradiance. Both the measurements and the calculations showed a drastic decrease in that layer, which could only be modeled using the measured profiles of the aerosol size distribution. With standard profiles for all input quantities, the considerable decrease in the UV irradiance within the hatched area cannot be reproduced. This is demonstrated by the dotted curve in Fig. 7a. It is calculated assuming the standard aerosol profiles from McClatchey et al. (1972) instead of our measurements. This shows that the decrease of radiation is

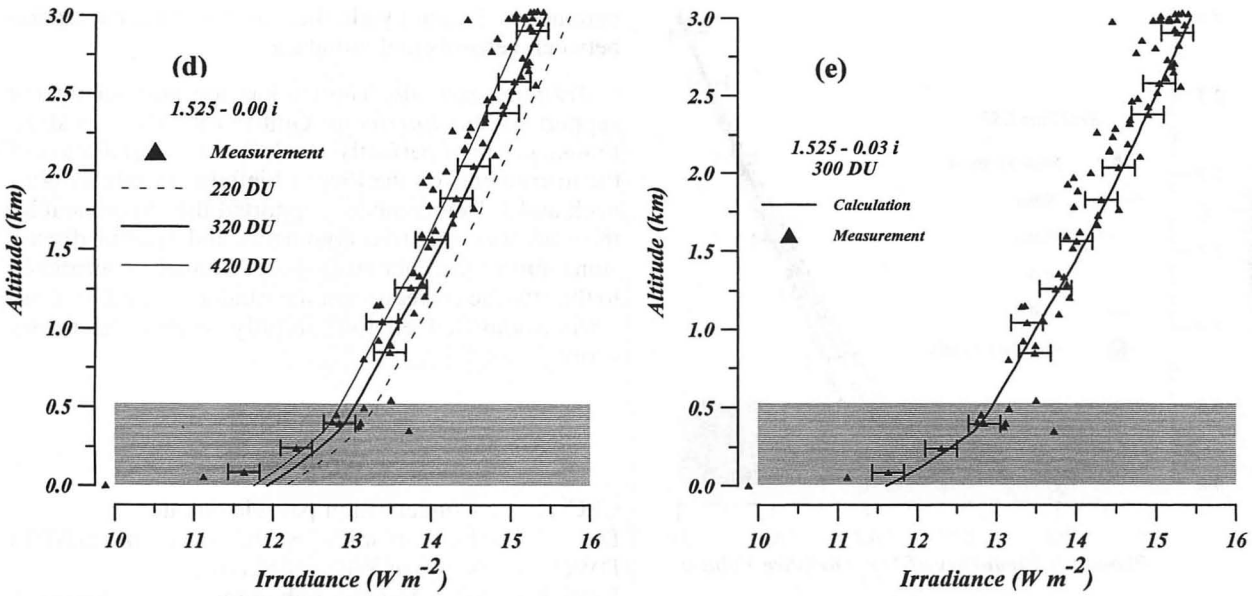

FIG. 7. (*Continued*)

a clear signal of direct aerosol influence on the downwelling UV irradiance.

The deviation of the calculated from the measured irradiance in the layer of enhanced aerosol concentration in Fig. 7a can be partly related to unrealistic treatment of aerosol absorption. In Fig. 7a the refractive index of ammonium sulfate was assumed, which is characterized by a very low imaginary part, that is very low absorption. In Fig. 7b the imaginary part of the refractive index was varied in the calculations. The result was an enhanced decrease of the downwelling irradiances especially in the hatched area. Thus, the agreement between measurement and calculation was improved, incorporating moderate absorption into the calculations. Changing the real part of the refractive index did not cause such drastic effects (Fig. 7c). The same statement holds for the ground albedo (not shown).

Another important parameter for the downward UV irradiances is the total amount of ozone. It can vary by 100 DU within a few days [cf. DWD Hohenpeissenberg reference in Ruggaber et al. (1994)]. This variation was simulated and the respective results are shown in Fig. 7d. The larger the total ozone content, the higher was the reduction of downward irradiance.

In Fig. 7e the results of the best fit in terms of minimum quadratic difference between measurement and calculation are presented. The important parameters (imaginary part of refractive index and total ozone content) were varied in a systematic way. A minimum difference between measurement and calculation was achieved using the refractive index of $n = 1.525 - 0.03i$ and a total ozone amount of 300 DU. The total amount of ozone agreed very well with measurements performed at the DWD stations in Hohenpeissenberg (24 November 1993: 287 DU) and Potsdam (24 November 1993; 309 DU, 1 December 1993: 298 DU). However, some minor discrepancies between measured and calculated irradiances near the ground remained.

b. Photolysis frequency of NO_2

Figure 8 shows the results for the photolysis frequency of NO_2. The comparison is based on relative values because of lack of reliable calibration data for the instrument. There are some differences between measurement and calculation. Uncertainties of both the measurements and calculations have contributed to the disagreement. Included in the figure are curves assuming different aerosol absorption in the radiative transfer calculations. Although the trend of decreasing photolysis frequency by increasing absorption is obvious, the agreement between measurement and calculation does not improve.

Despite the discrepancies, it can be concluded that the influence of the enhanced aerosol concentration on JNO_2 profiles was evident. Again, the measurements show a stronger decrease than the model, which can partly be attributed to higher absorption of the aerosol particles than assumed in the model. The dotted curve indicates the results of the simulations based on the standard aerosol profiles from McClatchey et al. (1972). The strong decrease of the downwelling radiation within the layer of enhanced aerosol concentration was not verified using standard assumptions for the aerosol.

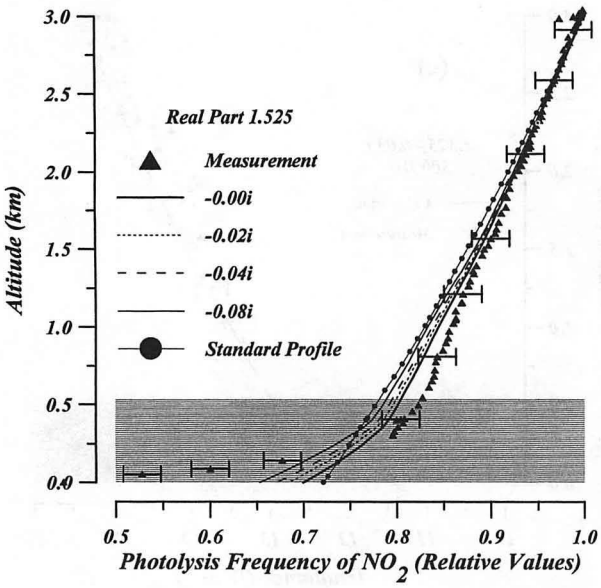

FIG. 8. Measurements of JNO_2 photolysis frequency and corresponding calculated values versus altitude for the ascent on 26 November 1993 near Mönchengladbach, Germany. The different curves show the results of the calculations based on measured profiles of meteorological and aerosol parameters (cf. Table 2). The dotted curve represents the calculations using standard aerosol assumptions as input for the model.

6. Conclusions

By using airborne aerosol and radiation measurements, a direct link between aerosol properties and resulting radiative quantities was established. An enhanced aerosol concentration caused by a temperature inversion layer drastically reduced the downwelling solar and UV irradiance, as well as the NO_2 photolysis frequency.

The measured aerosol size distributions were used to calculate different single-scattering properties of the particles. These calculations have shown that the aerosol stratification strongly influences the single-scattering properties considered (volume scattering coefficient σ_{sp}, asymmetry factor g, and backscattering ratio S). This implies that instead of simple aerosol concentration measurements, a description of the aerosol size distribution is required to derive a realistic picture of the optical conditions of the atmosphere.

The radiative transfer calculations confirmed the correlation between aerosol and radiative properties. The layer of enhanced number of optically efficient aerosol particles below the temperature inversion reduced the downward irradiance (solar and UV) and the JNO_2 photolysis frequency. This effect was evident in the measurements and in the results of the radiative transfer calculations. Therefore, detailed information on the aerosol size distribution need to be incorporated into model studies. Using simple assumptions for the input parameters does not yield the features of the interaction between aerosols and radiation.

Acknowledgments. The authors are grateful for the support of the *Enviscope* GmbH (R. Maser and H. Franke), which perfectly conducted the installation of the instruments on the Piper Chieftain aircraft. P. Warneck and J. Heintzenberg supported the experiment by their helpful scientific comments and fruitful discussions during the data analysis. L. Bannehr contributed to the attitude correction of the irradiance data. D. Covert is acknowledged for carefully reading the manuscript.

APPENDIX

Acronyms

CPC	Condensation particle counter
DU	Dobson unit (100 DU = 0.1 atm cm NPT)
DWD	German Weather Service
EPPLAB	The Eppley Laboratory, Inc., Newport, Rhode Island
GPS	Global positioning system
INS	Inertial navigation system
PCASP-X	Passive cavity aerosol spectrometer probe
PHA	Pulse height analyzer
PMS	Particle Measuring Systems, Inc., Boulder, Colorado
PSP	Precision spectral pyranometer (EPPLAB)
TSI	Thermosystems, Inc., St. Paul, Minnesota
TUVR	Ultraviolet radiometer (EPPLAB)

REFERENCES

Bannehr, L., and V. Glover, 1991: Preprocessing of airborne pyranometer data. NCAR Tech. Note NCAR/TN-364+STR, 35 pp.

——, and R. Schwiesow, 1993: A technique to account for the misalignment of pyranometers installed on aircraft. *J. Atmos. Oceanic Technol.,* **10,** 774–777.

Bohren, C. F., and D. R. Huffman, 1983: *The Absorption and Scattering of Light by Small Particles.* John Wiley & Sons, 530 pp.

Bowker, D. E., R. E. Davis, D. L. Myrick, K. Stacy, and W. T. Jones, 1985: Spectral reflectances of natural targets for use in remote sensing studies. NASA Ref. Publ. 1139.

Brock, C. A., L. F. Radke, J. H. Lyons, and P. V. Hobbs, 1989: Arctic hazes in summer over Greenland and the North American Arctic. I: Incidence and origins. *J. Atmos. Chem.,* **9,** 129–148.

Charlson, R. J., and T. M. L. Wigley, 1994: Sulfate aerosol and climate change. *Sci. Amer.,* **270,** 28–35.

d'Almeida, G., P. Koepke, and E. Shettle, 1991: *Atmospheric Aerosols, Global Climatology and Radiative Characteristics.* A. Deepak, 561 pp.

de Arellano, J. V., P. Dynkerke, and M. van Weele, 1994: Tethered-balloon measurements of actinic flux in a cloud-capped marine boundary layer. *J. Geophys. Res.,* **99,** 3699–3705.

Demerjian, K. L., K. L. Schere, and J. T. Peterson, 1980: Theoretical estimates of actinic (spherically integrated) flux and photolytic rate constants of atmospheric species in the lower troposphere. *Adv. Environ. Sci. Technol.,* **10,** 369–459.

Evans, B. T. N., 1988: Sensitivity of the backscatter/extinction ratio to changes in aerosol properties: Implications for lidar. *Appl. Opt.,* **27,** 3299–3305.

Finlayson-Pitts, B. J., and J. N. Pitts, 1986: *Atmospheric Chemistry: Fundamentals and Experimental Techniques.* Wiley, 1098 pp.

Foot, J. S., M. Kitchen, and C. J. Readings, 1985: The measurement of diffuse solar radiation from an aircraft. *Atmos. Environ.*, **19**, 811–818.

Grassl, H., 1988: Radiative effects of atmospheric aerosol particles. *Aerosol and Climate.* P. V. Hobbs and M. P. McCormick, Eds., A. Deepack Publishing, 241–252.

Gunter, R. L., A. D. A. Hansen, J. F. Boatman, B. A. Bodhaine, R. C. Schnell, and D. M. Garvey, 1993: Airborne measurements of aerosol optical properties over the south-central New Mexico. *Atmos. Environ.*, **27A**, 1363–1368.

Horvath, H., 1991: Spectral extinction coefficients of background aerosols in Europe, North and South America: A comparison. *Atmos. Environ.*, **25A**, 725–732.

Iqbal, M., 1983: *An Introduction to Solar Radiation.* Academic Press, 390 pp.

Junkermann, W., and U. Platt, 1989: A photoelectric detector for the measurement of photolysis frequencies of ozone and other atmospheric molecules. *J. Atmos. Chem.*, **8**, 203–227.

Kilsby, C. G., 1990: A study of aerosol properties and solar radiation during a straw-burning episode using aircraft and satellite measurements. *Quart. J. Roy. Meteor. Soc.*, **116**, 1173–1192.

Kim, Y. J., J. F. Boatman, R. L. Gunter, D. L. Wellman, and S. W. Wilkison, 1993: Vertical distribution of atmospheric aerosol size distribution over the south-central New Mexico. *Atmos. Environ.*, **27A**, 1351–1362.

Kristament, I. S., J. B. Liley, and M. J. Harvey, 1993: Aerosol variability in the vertical in the Southwest Pacific. *J. Geophys. Res.*, **98**, 7129–7139.

Madronich, S., 1987: Photodissociation in the atmosphere. 1. Actinic flux and the effects of ground reflections and clouds. *J. Geophys. Res.*, **92**, 9740–9752.

Maser, R., H. Franke, M. Preiss, and W. Jaeschke, 1994: Methods provided and applied in a research aircraft for the study of cloud physics and chemistry. *Contrib. Atmos. Phys.*, **67**, 321–334.

McClatchey, R. A., R. W. Fenn, J. E. A. Selby, F. E. Volz, and J. S. Garing, 1972: Optical properties of the atmosphere. AFCRL-72-0497, Environmental Research Papers, 411 pp.

Nakajima, T., and M. Tanaka, 1986: Matrix formulations for the transfer of solar radiation in a plane-parallel scattering atmosphere. *J. Quant. Spectrosc. Radiat. Transfer*, **35**, 13–21.

——, and ——, 1988: Algorithms for radiative intensity calculations in moderately thick atmospheres using a truncation approximation. *J. Quant. Spectrosc. Radiat. Transfer*, **40**, 51–69.

Roeth, E.-P., 1986: Description of one-dimensional model for atmospheric chemistry. *Ber. Kernforschungsanlage Juelich*, p. 2098.

Ruggaber, A., R. Dlugi, and T. Nakajima, 1994: Modelling radiation quantities and photolysis frequencies in the troposphere. *J. Atmos. Chem.*, **18**, 171–210.

Saunders, R. W., G. Brogniez, J. C. Buriez, R. Meerkötter, and P. Wendling, 1992: A comparison of measured and modeled broadband fluxes from aircraft data during the ICE'89 field experiment. *J. Atmos. Oceanic Technol.*, **9**, 391–406.

Stettler, M., and W. von Hoyningen-Huene, 1994: Three years of aerosol extinction measurements with a He.Ne-laser in the urban boundary layer of Leipzig, Germany. *Contrib. Atmos. Phys.*, **67**, 169–180.

Tanaka, M., T. Hayasaka, and T. Nakajima, 1990: Airborne measurements of optical properties of tropospheric aerosols over an urban area. *J. Meteor. Soc. Japan*, **68**, 335–345.

Tang, I. N., and H. R. Munkelwitz, 1993: Composition and temperature dependence of the deliquescence properties of hygroscopic aerosols. *Atmos. Environ.*, **27A**, 467–473.

van Weele, M., and P. G. Duynkerke, 1993: Effects of clouds on the photodissociation of NO_2: Observations and modelling. *J. Atmos. Chem.*, **16**, 231–255.